

One-Way Topological States along Vague Boundaries in Synthetic Frequency Dimensions including Group Velocity Dispersion

Qingrou Shan¹, Danying Yu¹, Guangzhen Li¹, Luqi Yuan^{1, *}, and Xianfeng Chen^{1, 2, 3}

(Invited)

Abstract—We recently proposed a two-dimensional synthetic space including one spatial axis and one synthetic frequency dimension in a one-dimensional ring resonator array [*Opt. Lett.*, Vol. 41, No. 4, 741–744, 2016]. Nevertheless, the group velocity dispersion (GVD) of the waveguides that compose rings was ignored for simplicity. In this paper, we extend the previous work and study the topological one-way edge states in such a synthetic space involving GVD. We show that the GVD brings a natural vague boundary in the frequency dimension, so the topological edge state still propagates at several frequency modes unidirectionally along the spatial axis. Positions of such vague boundary can be controlled by changing the magnitude of the GVD. In particular, a relatively strong GVD can degrade this two-dimensional synthetic space to one-dimensional spatial lattice, but yet the one-way state is still preserved in simulations. Our work therefore exhibits the impact of the GVD on topological photonics in the synthetic space, which will be important for future practical experimental implementations.

1. INTRODUCTION

Topological photonics has been drawing remarkable attention in the photonic society over the past decade [1–4]. Various kinds of photonic platforms have been exploited to study the topological physics in photonics, including systems of coupled optical waveguides [5–10], arrays of ring resonators [11–15], photonic crystals [16–20], and metamaterials [21]. Potential applications of topological photonics lead to extensive achievements in photonic devices like topologically protected unidirectional waveguides [22–25], topological fiber [26], topological lasing [12, 27, 28], and topological optical switches [29].

Besides achieving topological photonics in systems with real dimensions, recent developments of topology in synthetic space are of great significance [30, 31]. In photonics, synthetic dimensions can be constructed by using diverse photonic freedoms such as photonic modes carrying different frequencies [32–37], different orbital angular momentums of light [38–40], and multiple pulses utilizing the temporal degree of freedom [41–45], which therefore provide many novel opportunities for exploring interesting physics along the synthetic dimension. Several experiments have been carried out successfully to demonstrate synthetic dimensions [34, 35, 42, 46] and also study the topological photonics in synthetic spaces [45, 47, 48]. Among these platforms, the ring resonators consisting of optical fibers or photonic waveguides have been shown to be a good candidate to create the synthetic frequency dimension. But yet, the relation between the boundary along the frequency axis of light and the group velocity dispersion (GVD) of the materials in the rings is still unclear.

In our work, we explore a two-dimensional synthetic space, including the frequency axis of light without artificial frequency boundaries, in a one-dimensional ring resonator array constructed by

Received 31 August 2020, Accepted 20 November 2020, Scheduled 30 November 2020

* Corresponding author: Luqi Yuan (yuanluqi@sjtu.edu.cn).

¹ State Key Laboratory of Advanced Optical Communication Systems and Networks, School of Physics and Astronomy, Shanghai Jiao Tong University, Shanghai 200240, China. ² Jinan Institute of Quantum Technology, Jinan 250101, China. ³ Collaborative Innovation Center of Light Manipulation and Applications, Shandong Normal University, Jinan 250358, China.

dispersive waveguides. In such a two-dimensional synthetic space, the distribution of modulation phases in each ring is chosen to create the synthetic magnetic field for photons [32, 33]. We show that even without boundary in the frequency dimension, the topological edge state of the field can still propagate within some frequency modes unidirectionally along the spatial dimension, which therefore gives a vague boundary in the frequency dimension due to the effect from the GVD. The range of the vague boundary is related to the magnitude of the GVD. We find that, as the GVD increases, the effective range of the frequency dimension narrows down to only two columns, where the topological edge state is still preserved. Our work explores the impact of the GVD on topological photonics in the synthetic space, which is important for future studies from experimental aspects.

2. THEORETICAL MODEL

We start with considering a one-dimensional ring resonator array, composed of 5 coupled ring resonators which carry electro-optic modulators (EOM) as shown in Fig. 1(a). Each ring is undergoing the dynamic modulation with the modulation frequency Ω and modulation phase ψ_n , with n being the integer labelling the ring. The ring resonator supports a set of resonant modes. Without the GVD, the frequencies of resonant modes are equally spaced with the frequency interval being the free-spectral-range Ω_R . If one chooses $\Omega = \Omega_R$, modulations in each ring form sideband generations at the frequency ω_m :

$$\omega_m = \omega_0 + m\Omega, \quad (1)$$

where m is an integer to label the m -th resonant mode, and ω_0 is defined as the resonant frequency at the zero GVD point. Since the sideband frequency matches with the resonant frequency in the ring, the modulation connects the nearby resonant modes and forms the synthetic frequency dimension. In the weak modulation limit, the system therefore supports a synthetic two-dimensional square lattice including both the spatial and frequency dimensions as shown in Fig. 1(b). If the modulation phases are chosen to be $\psi_n = n\pi/2$, there exists an effective magnetic field in the synthetic space, which generates topological edge states [32].

Nevertheless, in practical experiments, the ring resonators consist of waveguides having the GVD, which is taken into account here. The single-mode waveguide in each ring resonator has the dispersion

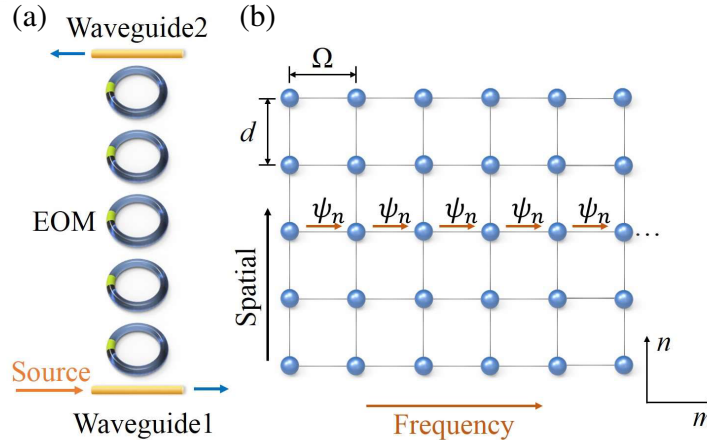


Figure 1. (a) A one-dimensional ring resonator array with 5 ring resonators carrying electro-optic modulators (EOM) which are marked green. External waveguide 1 and waveguide 2 are coupled to the bottom and the top ring resonator, respectively. The source imports through waveguide 1 while output spectra get collected through both waveguide 1 and waveguide 2. (b) The two-dimensional synthetic space with the vertical axis being the spatial dimension and the horizontal axis being the frequency dimension.

relation

$$\beta(\omega) = n(\omega) \frac{\omega}{c}, \quad (2)$$

where β is the propagation wavevector along the light propagation direction (which is defined as the z -direction) inside the waveguide. $n(\omega)$ represents the effective refractive index. If we consider the GVD, $n(\omega)$ is not a constant. Hence the modulation frequency is no longer resonant with the frequency spacing between two nearby resonant modes, and frequencies of the sideband generation (at ω_m near ω_0) due to modulations are also not equal to the resonant frequencies [33, 49]. For light propagating after one round-trip in such a ring modulated near ω_0 , the frequency mismatching from the GVD for each resonant mode results in the situation that the field accumulates an additional phase, which is not a multiple of 2π , i.e.,

$$\varphi_m = [\beta(\omega_m) - \beta(\omega_0)] L \neq m \cdot 2\pi. \quad (3)$$

Here L is the length of the ring. We use the fused silica as an example and take the Sellmeier equation given in [50]. In Fig. 2, we plot $\varphi_m/2\pi$ near the center wavelength at $1.27 \mu\text{m}$ with the modulation frequency $\Omega = 100 \text{ MHz}$ and $L = 13 \text{ m}$. One can see that the phase offset $\Delta_m \equiv \varphi_m/2\pi - m$ for the m -th mode becomes much more significant when the mode number m is larger.

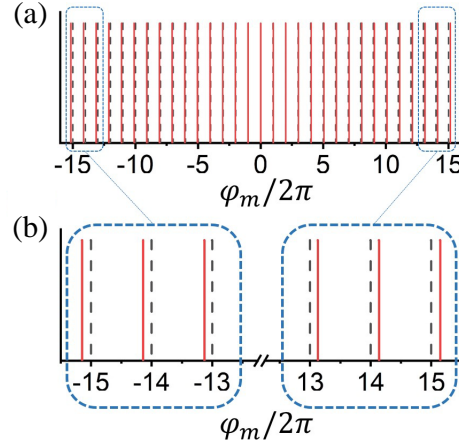


Figure 2. (a) Additional phases φ_m accumulated around the center wavelength at $1.27 \mu\text{m}$, with $\Omega = 100 \text{ MHz}$, $L = 13 \text{ m}$, and $m = -15, \dots, 15$ for fused silica [50]. (b) Zoomed-in phases $\varphi_m/2\pi$ for $m = \pm 13, \pm 14$ and ± 15 , respectively.

In the following, we briefly introduce the numerical formula [32, 51] that we use to study the propagation of topological edge modes in the synthetic space including the phase offset due to the GVD. We consider 5 rings ($n = 1, \dots, 5$) coupled with two waveguides as shown in Fig. 1(a). In each ring resonator, we expand the electric field by the sideband components as

$$E(t, r_{\perp}, z) = \sum_m \mathcal{E}_m(t, z) E_m(r_{\perp}) e^{i\omega_m t}, \quad (4)$$

where r_{\perp} expresses the directions orthogonal to z . $E_m(r_{\perp})$ is the modal profile, and $\mathcal{E}_m(t, z)$ is its amplitude at the m -th sideband. The modal amplitude follows Maxwell's equations and satisfies the wave propagation equation by introducing the slow-varying-envelope approximation [52]

$$\left(\frac{\partial}{\partial x} + i\beta(\omega_m) \right) \mathcal{E}_m(t, z) - \frac{n_g(\omega_m)}{c} \frac{\partial}{\partial t} \mathcal{E}_m(t, z) = 0. \quad (5)$$

There exists a natural periodic boundary as $\mathcal{E}_m(t, z + L) = \mathcal{E}_m(t, z)$ while the field circulates in the ring. Hence $\beta(\omega_m)$ results in the phase offset Δ_m which makes the m -th frequency component cannot be accumulated constructively during each round-trip propagation.

The coupling of the fields between two nearest n -th and $(n+1)$ -th ring resonators can be described by [53, 54]

$$\mathcal{E}_m^n(t^+, z_T^n) = \sqrt{1 - \gamma^2} \mathcal{E}_m^n(t^-, z_T^n) - i\gamma \mathcal{E}_m^{n+1}(t^-, z_B^{n+1}), \quad (6)$$

$$\mathcal{E}_m^{n+1}(t^+, z_B^{n+1}) = \sqrt{1 - \gamma^2} \mathcal{E}_m^{n+1}(t^-, z_B^{n+1}) - i\gamma \mathcal{E}_m^n(t^-, z_T^n). \quad (7)$$

Here z_T^n and z_B^{n+1} are the top point of the n -th ring and the bottom point of the $(n+1)$ -th ring, marking the position where the coupling occurs. γ is the coupling strength between resonators, and $t^\pm = t + 0^\pm$.

Two waveguides coupled with two rings at the spatial boundary are used for the input and output purpose, which follows the input-output equations [55, 56]:

$$\mathcal{E}_m^1(t^+, z_B^1) = \sqrt{1 - \eta^2} \mathcal{E}_m^1(t^-, z_B^1) - i\eta E_m^{\text{in}}(t^-), \quad (8)$$

$$E_{m,B}^{\text{out}}(t^+) = \sqrt{(1 - \eta^2)} E_m^{\text{in}}(t^-) + i\eta \mathcal{E}_m^1(t^-, z_B^1), \quad (9)$$

$$E_{m,T}^{\text{out}}(t^+) = i\eta \mathcal{E}_m^5(t^-, z_T^5), \quad (10)$$

where E_m^{in} and $E_{m,B/T}^{\text{out}}$ represent the input source field and output field at the bottom/top waveguide for the m -th frequency component, respectively. η is the coupling strength between the resonator and the waveguide.

We allocate the EOM at z_{EOM}^n to induce the sinusoidal dynamic modulation in the n -th ring resonator. The change of the field follows the standard Bessel expansion [32, 51, 57]

$$\begin{aligned} \mathcal{E}_m^n(t^+, z_{\text{EOM}}^n) &= J_0(\alpha) \mathcal{E}_m^n(t^-, z_{\text{EOM}}^n) + \sum_l J_l(\alpha) \mathcal{E}_{m-l}^n(t^-, z_{\text{EOM}}^n) e^{il\psi_n} \\ &\quad + \sum_l (-1)^l J_l(\alpha) \mathcal{E}_{m+l}^n(t^-, z_{\text{EOM}}^n) e^{-il\psi_n}, \end{aligned} \quad (11)$$

where J_l is the l -th order Bessel function, and α is the modulation strength. For $\alpha \ll 1$, the system is weakly modulated, and one has the approximation that $J_0(\alpha) \approx 1$ and $J_{\pm 1}(\alpha) \approx \alpha/2$, with other orders of Bessel components being approximately zero.

3. SIMULATIONS AND RESULTS

We perform simulations on this one-dimensional ring resonator array as shown in Fig. 1(a). The ring resonator array is composed of 5 rings, each of which is modulated with the phase $\psi_n = n\pi/2$. Moreover, we choose 31 sideband modes in each ring in simulations, with $m = -15, \dots, 15$. Such a platform supports a 5×31 synthetic lattice in the synthetic space [see Fig. 1(b)]. The GVD is considered which causes the phase offset Δ_m as shown in Fig. 2. The single-frequency input field is injected through the input waveguide at the bottom of the ring array, while the output signals can be collected at both waveguides. Eqs. (5)–(11) are used to perform the simulations with parameters $\alpha = 0.456$, $\gamma = 0.224\Omega/2\pi$, and $\eta = 0.071\Omega/2\pi$. The input source has a frequency near ω_0 with a small detuning $\sim 2J_1(\alpha)\Omega/2\pi$, which is chosen to selectively excite the topological edge states [32]. Moreover, an intrinsic loss γ_i is added, so we can tune this parameter and find the steady-state field propagation with different losses.

In Fig. 3, we plot distributions of intensities of sideband modes in all 5 rings in the steady-state regime in simulations, together with the spectra of the output fields $|E_B^{\text{out}}|^2$ and $|E_T^{\text{out}}|^2$ through the two waveguides. The intrinsic loss γ_i is chosen to be $4\pi^2\gamma_i^2/\Omega^2 = 0.04, 0.02, \text{ and } 0$, respectively. We can clearly see that the intensity of the field has a clockwise-propagation tendency while γ_i is decreasing. The field starts from the bottom center of the synthetic lattice and propagates towards lower modes in the 1st ring. Such conversion vaguely stops near the -5 th mode, and the field transfers from the 1st ring to the 5th ring through several modes near the -5 th mode. Moreover, from output spectra, one sees that $|E_B^{\text{out}}|^2$ in the bottom waveguide gives the frequency conversion to the lower frequency components. On the other hand, $|E_T^{\text{out}}|^2$ in the top waveguide shows a peak at $m = -5$, indicating that the transfer of the field at the vague boundary happens at modes near $m = -5$. Once the field reaches the top boundary, it starts the frequency conversion towards higher modes. As a comparison, we also

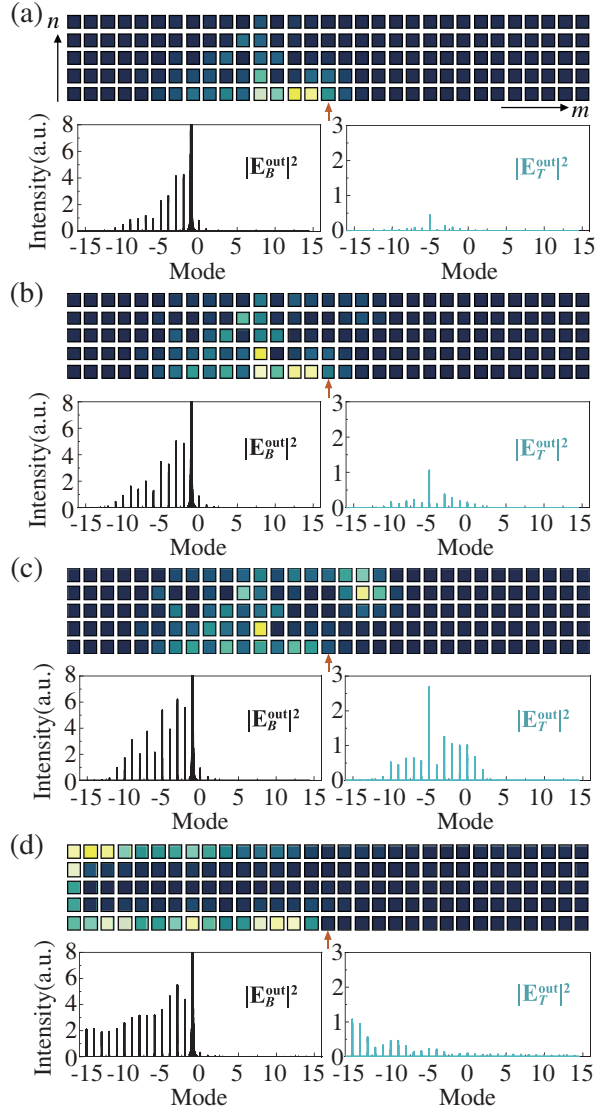


Figure 3. Distribution of intensity of sideband modes in the 5×31 synthetic lattice and the corresponding spectra of the output fields $|E_B^{\text{out}}|^2$ and $|E_T^{\text{out}}|^2$ through the two waveguides, with the phase offset Δ_m given in Fig. 2, and (a) $4\pi^2\gamma_i^2/\Omega^2 = 0.04$, (b) $4\pi^2\gamma_i^2/\Omega^2 = 0.02$, (c) $4\pi^2\gamma_i^2/\Omega^2 = 0$, (d) phase offset being zero and $4\pi^2\gamma_i^2/\Omega^2 = 0$, respectively in simulations. Orange arrow indicates that the 0th mode at the 1st ring is excited by the external source.

show distributions of intensities in such a synthetic lattice without considering GVD in Fig. 3(d) (i.e., phase offset being zero, under the condition $4\pi^2\gamma_i^2/\Omega^2 = 0$), where one can see the expected edge mode around the real spatial boundary as well as the artificially-set spectral boundary at $m = -15$ [32]. Thus, the unidirectional propagation of the edge state in such a synthetic space elucidates that the frequency mismatching from the GVD can induce the vague boundary at the synthetic frequency dimension, where the topological photonics properties still exhibit.

We can arbitrarily change the phase offset to explore the dynamics in the synthetic lattice with the vague boundary. We first set $\Delta_m^{(1)} = (\varphi_m/2\pi - m)/2 = \Delta_m/2$, which gives the half phase offset compared with Δ_m in the previous case. Fig. 4 plots the distributions of intensities of sideband modes and the intensity spectra of the output fields with the offset $\Delta_m^{(1)}$ and all other parameters being the same as those in the previous case. One can still see the one-way propagation in the synthetic lattice,

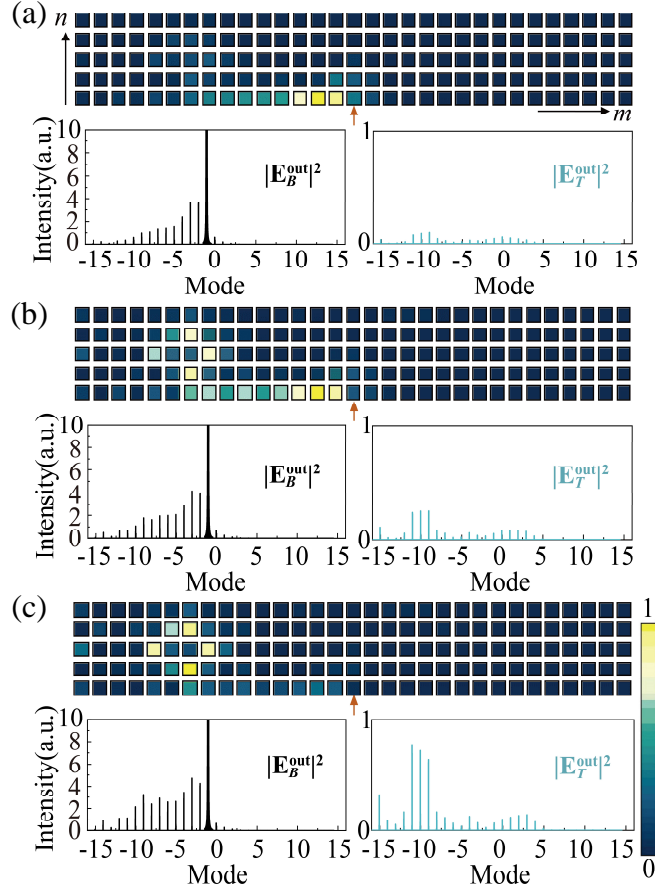


Figure 4. Distribution of intensity of sideband modes in the 5×31 synthetic lattice, and the corresponding spectra of the output fields $|E_B^{\text{out}}|^2$ and $|E_T^{\text{out}}|^2$ through the two waveguides, with the phase offset $\Delta_m^{(1)}$, and (a) $4\pi^2\gamma_i^2/\Omega^2 = 0.04$, (b) $4\pi^2\gamma_i^2/\Omega^2 = 0.02$, (c) $4\pi^2\gamma_i^2/\Omega^2 = 0$, respectively in simulations. Orange arrow indicates that the 0th mode at the 1st ring is excited by the external source.

yet the vague boundary is shifted. Peaks around $m = -10$ are shown in the output spectra $|E_T^{\text{out}}|^2$. The effective area is broadened since the offset from the GVD is smaller. Hence, the choice of the material GVD can be used to control where the vague boundary is at the frequency axis that the light of one-way edge mode transports though in the synthetic lattice.

Similarly, one can also set the phase offset to be $\Delta_m^{(2)} \equiv 2(\varphi_m/2\pi - m) = 2\Delta_m$ but keep the other parameters unchanged in simulations. The corresponding distributions of intensities of sideband modes and the intensity spectra of the output fields are shown in Fig. 5. Besides the one-way edge mode exhibits in the synthetic lattice, the vague boundary is shifted in the opposite direction as compared with plots in Fig. 4 for $\Delta_m^{(1)}$. In simulations, both vague boundaries at the negative and positive frequency axes can be seen in the intensity distribution in the simulation with $4\pi^2\gamma_i^2/\Omega^2 = 0$. Larger choice of the material GVD therefore decreases the effective area in the synthetic lattice.

It is interesting to explore what is the limit condition for changing vague boundary to shrink the effective area in the synthetic space. Hence, we set $\Delta_m^{(3)} \equiv 10(\varphi_m/2\pi - m) = 10\Delta_m$ and $\Delta_m^{(4)} \equiv 20(\varphi_m/2\pi - m) = 20\Delta_m$, respectively. The other parameters are still chosen to be the same, but the intrinsic loss is set as $4\pi^2\gamma_i^2/\Omega^2 = 0.08, 0.04, \text{ and } 0$, respectively. The distributions of intensities of the sideband modes are shown in Fig. 6. In Figs. 6(a)–6(c), for increased magnitude of GVD with the offset $\Delta_m^{(3)}$, the clockwise one-way edge state remains explicit but in the synthetic frequency dimension persisting merely in two columns. The intensity of the field propagates towards one sideband mode left

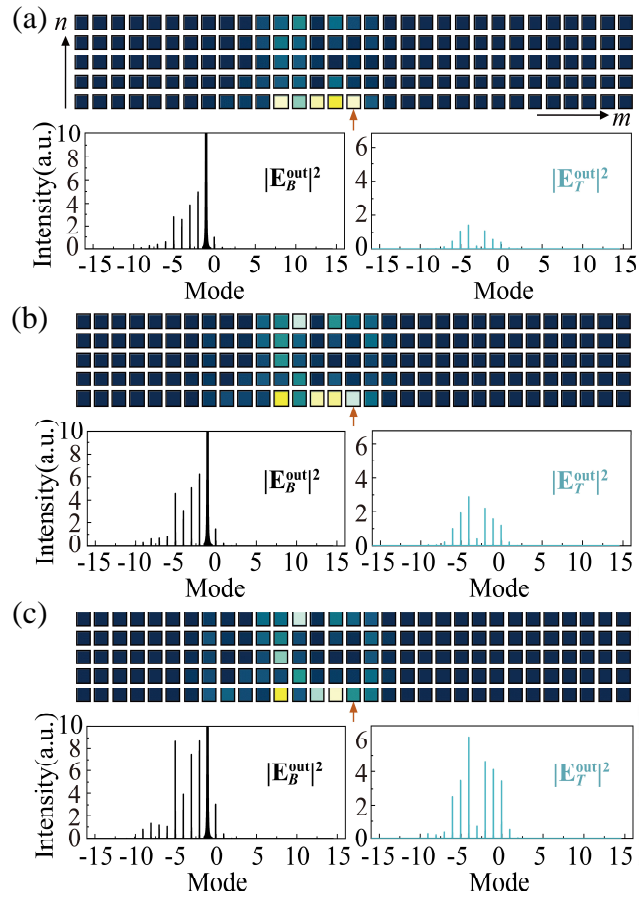


Figure 5. Distribution of intensity of sideband modes in the 5×31 synthetic lattice and the corresponding spectra of the output fields $|E_B^{\text{out}}|^2$ and $|E_T^{\text{out}}|^2$ through the two waveguides, with the phase offset $\Delta_m^{(2)}$, and (a) $4\pi^2\gamma_i^2/\Omega^2 = 0.04$, (b) $4\pi^2\gamma_i^2/\Omega^2 = 0.02$, (c) $4\pi^2\gamma_i^2/\Omega^2 = 0$, respectively in simulations. Orange arrow indicates that the 0th mode at the 1st ring is excited by the external source.

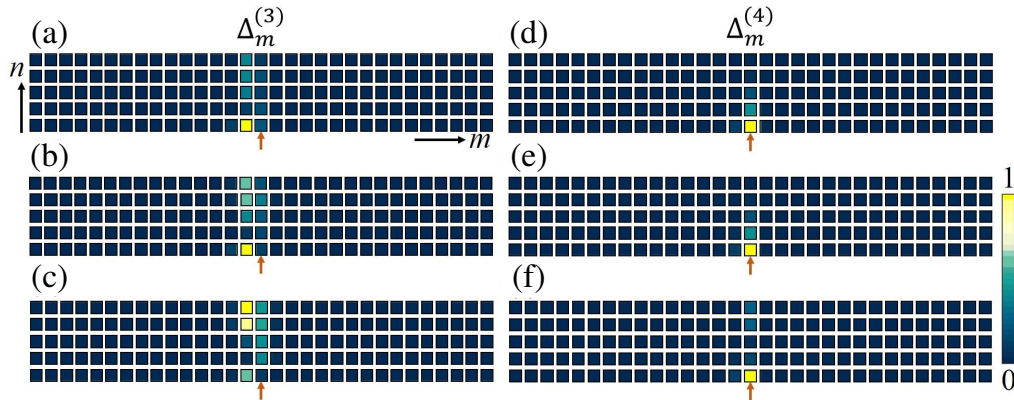


Figure 6. Distribution of intensity of sideband modes in the 5×31 synthetic lattice. The phase offset is $\Delta_m^{(3)}$ for the left panel and (a) $4\pi^2\gamma_i^2/\Omega^2 = 0.08$, (b) $4\pi^2\gamma_i^2/\Omega^2 = 0.04$, (c) $4\pi^2\gamma_i^2/\Omega^2 = 0$, respectively, while the phase offset is $\Delta_m^{(4)}$ for the right panel and (d) $4\pi^2\gamma_i^2/\Omega^2 = 0.08$, (e) $4\pi^2\gamma_i^2/\Omega^2 = 0.04$, (f) $4\pi^2\gamma_i^2/\Omega^2 = 0$, respectively in the simulations. Orange arrow indicates that the 0th mode at the 1st ring is excited by the external source.

from the initial excitation mode, then it directly propagates along the spatial dimension to the upper side of the lattice, and afterwards it bounces back. On the other hand, for an even larger GVD with the offset $\Delta_m^{(4)}$, the propagation of the edge state at the vague boundary in a two-dimensional synthetic lattice disappears, as shown in Figs. 6(d)–6(f). The synthetic frequency dimension fades away, so the field propagates only at the 0th mode in spatial direction. However, it is interesting to see that, in this effective one-dimensional lattice, the energy is mostly localized at the 0th sideband mode in the 1st ring, but the propagation still shows one-way directionality towards the 5th ring. Thus, for a relatively large GVD, the synthetic frequency dimension breaks, and one cannot construct an effective two-dimensional synthetic space.

4. CONCLUSION

In summary, we work on a synthetic lattice including both spatial and frequency dimensions, where an effective gauge field can be prepared [32], and study the topological one-way edge modes under the effect of the GVD. The GVD provides a natural vague boundary at the frequency dimension, so the one-way edge mode of the light can propagate unidirectionally along the spatial axis without an artificial boundary prepared at the frequency dimension. Magnitudes of the GVD can be used to control the effective area in the synthetic lattice. In particular, a relatively large GVD breaks the synthetic frequency dimension. Our work is important for further experimental studies of the synthetic frequency dimension based on either fiber loops [46, 48] or lithium niobate on-chip implementations [58, 59].

ACKNOWLEDGMENT

The research is supported by the National Natural Science Foundation of China (11974245), National Key R&D Program of China (2017YFA0303701), Shanghai Municipal Science and Technology Major Project (2019SHZDZX01), Natural Science Foundation of Shanghai (19ZR1475700), and China Postdoctoral Science Foundation (2020M671090). X. C. also acknowledges the support from Shandong Quancheng Scholarship (00242019024).

REFERENCES

1. Lu, L., J. D. Joannopoulos, and M. Soljačić, “Topological photonics,” *Nature Photonics*, Vol. 8, No. 11, 821–829, 2014.
2. Khanikaev, A. B. and G. Shvets, “Two-dimensional topological photonics,” *Nature Photonics*, Vol. 11, No. 12, 763–773, 2017.
3. Ozawa, T., H. M. Price, A. Amo, N. Goldman, M. Hafezi, L. Lu, M. C. Rechtsman, D. Schuster, J. Simon, O. Zilberberg, and I. Carusotto, “Topological photonics,” *Reviews of Modern Physics*, Vol. 91, No. 1, 015006, 2019.
4. Leykam, D. and L. Yuan, “Topological phases in ring resonators: Recent progress and future prospects,” *Nanophotonics*, Vol. 9, No. 15, 4473, 2020.
5. Kraus, Y. E., Y. Lahini, Z. Ringel, M. Verbin, and O. Zilberberg, “Topological states and adiabatic pumping in quasicrystals,” *Physical Review Letters*, Vol. 109, No. 10, 106402, 2012.
6. Rechtsman, M. C., J. M. Zeuner, Y. Plotnik, Y. Lumer, D. Podolsky, F. Dreisow, S. Nolte, M. Segev, and A. Szameit, “Photonic Floquet topological insulators,” *Nature*, Vol. 496, No. 7444, 196–200, 2013.
7. Weimann S., M. Kremer, Y. Plotnik, Y. Lumer, S. Nolte, K. G. Makris, M. Segev, M. C. Rechtsman, and A. Szameit, “Topologically protected bound states in photonic parity-time-symmetric crystals,” *Nature Materials*, Vol. 16, No. 4, 433–438, 2017.
8. Noh, J., S. Huang, D. Leykam, Y. D. Chong, K. P. Chen, and M. C. Rechtsman, “Experimental observation of optical Weyl points and Fermi arc-like surface states,” *Nature Physics*, Vol. 13, No. 6, 611–617, 2017.

9. Stützer, S., Y. Plotnik, Y. Lumer, P. Titum, N. H. Lindner, M. Segev, M. C. Rechtsman, and A. Szameit, "Photonic topological Anderson insulators," *Nature*, Vol. 560, No. 7719, 461–465, 2018.
10. Noh, J., S. Huang, K. P. Chen, and M. C. Rechtsman, "Observation of photonic topological valley hall edge states," *Physical Review Letters*, Vol. 120, No. 6, 063902, 2018.
11. Hafezi, M., S. Mittal, J. Fan, A. Migdall, and J. M. Taylor, "Imaging topological edge states in silicon photonics," *Nature Photonics*, Vol. 7, No. 12, 1001–1005, 2013.
12. Bandres, M. A., S. Wittek, G. Harari, M. Parto, J. Ren, M. Segev, D. N. Christodoulides, and M. Khajavikhan, "Topological insulator laser: Experiments," *Science*, Vol. 359, No. 6381, eaar4005, 2018.
13. Leykam, D., S. Mittal, M. Hafezi, and Y. D. Chong, "Reconfigurable topological phases in next-nearest-neighbor coupled resonator lattices," *Physical Review Letters*, Vol. 121, No. 2, 023901, 2018.
14. Mittal, S., V. V. Orre, G. Zhu, M. A. Gorlach, A. Poddubny, and M. Hafezi, "Photonic quadrupole topological phases," *Nature Photonics*, Vol. 13, No. 10, 692–696, 2019.
15. Mittal, S., V. V. Orre, D. Leykam, Y. D. Chong, and M. Hafezi, "Photonic anomalous quantum Hall effect," *Physical Review Letters*, Vol. 123, No. 4, 043201, 2019.
16. Wang, Z., Y. Chong, J. D. Joannopoulos, and M. Soljačić, "Observation of unidirectional backscattering-immune topological electromagnetic states," *Nature*, Vol. 461, No. 7265, 772–775, 2009.
17. Lu, L., Z. Wang, D. Ye, L. Ran, L. Fu, J. D. Joannopoulos, and M. Soljačić, "Experimental observation of Weyl points," *Science*, Vol. 349, No. 6248, 622, 2015.
18. Gao, F., H. Xue, Z. Yang, K. Lai, Y. Yu, X. Lin, Y. Chong, G. Shvets, and B. Zhang, "Topologically protected refraction of robust kink states in valley photonic crystals," *Nature Physics*, Vol. 14, No. 2, 140–144, 2018.
19. Yang, B., Q. Guo, B. Tremain, R. Liu, L. E. Barr, Q. Yan, W. Gao, H. Liu, Y. Xiang, J. Chen, C. Fang, A. Hibbins, L. Lu, and S. Zhang, "Ideal Weyl points and helicoid surface states in artificial photonic crystal structures," *Science*, Vol. 359, No. 6379, 1013, 2018.
20. Yang, Y., Z. Gao, H. Xue, L. Zhang, M. He, Z. Yang, R. Singh, Y. Chong, B. Zhang, and H. Chen, "Realization of a three-dimensional photonic topological insulator," *Nature*, Vol. 565, No. 7741, 622–626, 2019.
21. Khanikaev, A. B., S. Hossein Mousavi, W.-K. Tse, M. Kargarian, A. H. MacDonald, and G. Shvets, "Photonic topological insulators," *Nature Materials*, Vol. 12, No. 3, 233–239, 2013.
22. Fu, J.-X., R.-J. Liu, and Z.-Y. Li, "Robust one-way modes in gyromagnetic photonic crystal waveguides with different interfaces," *Applied Physics Letters*, Vol. 97, No. 4, 041112, 2010.
23. Poo, Y., R.-X. Wu, Z. Lin, Y. Yang, and C. T. Chan, "Experimental realization of self-guiding unidirectional electromagnetic edge states," *Physical Review Letters*, Vol. 106, No. 9, 093903, 2011.
24. Skirlo, S. A., L. Lu, Y. Igarashi, Q. Yan, J. Joannopoulos, and M. Soljačić, "Experimental observation of large chern numbers in photonic crystals," *Physical Review Letters*, Vol. 115, No. 25, 253901, 2015.
25. Blanco-Redondo, A., I. Andonegui, M. J. Collins, G. Harari, Y. Lumer, M. C. Rechtsman, B. J. Eggleton, and M. Segev, "Topological optical waveguiding in silicon and the transition between topological and trivial defect states," *Physical Review Letters*, Vol. 116, No. 16, 163901, 2016.
26. Lu, L., H. Gao, and Z. Wang, "Topological one-way fiber of second Chern number," *Nature Communications*, Vol. 9, No. 1, 5384, 2018.
27. Pilozzi, L. and C. Conti, "Topological lasing in resonant photonic structures," *Physical Review B*, Vol. 93, No. 19, 195317, 2016.
28. Zhang, W., X. Xie, H.-M. Hao, J. Dang, S. Xiao, S. Shi, H.-Q. Ni, Z. Niu, C. Wang, K. Jin, X. Zhang, and X. Xu, "Low-threshold topological nanolasers based on the second-order corner state," *Light, Science & Applications*, Vol. 9, 2020.

29. Leykam, D. and Y. D. Chong, “Edge solitons in nonlinear-photonic topological insulators,” *Physical Review Letters*, Vol. 117, No. 14, 143901, 2016.
30. Yuan, L., Q. Lin, M. Xiao, and S. Fan, “Synthetic dimension in photonics,” *Optica*, Vol. 5, No. 11, 1396–1405, 2018.
31. Ozawa, T. and H. M. Price, “Topological quantum matter in synthetic dimensions,” *Nature Reviews Physics*, Vol. 1, No. 5, 349–357, 2019.
32. Yuan, L., Y. Shi, and S. Fan, “Photonic gauge potential in a system with a synthetic frequency dimension,” *Opt. Lett.*, Vol. 41, No. 4, 741–744, 2016.
33. Ozawa, T., H. M. Price, N. Goldman, O. Zilberberg, and I. Carusotto, “Synthetic dimensions in integrated photonics: From optical isolation to four-dimensional quantum Hall physics,” *Physical Review A*, Vol. 93, No. 4, 043827, 2016.
34. Bell, B. A., K. Wang, A. S. Solntsev, D. N. Neshev, A. A. Sukhorukov, and B. J. Eggleton, “Spectral photonic lattices with complex long-range coupling,” *Optica*, Vol. 4, 1433–1436, 2017.
35. Qin, C., F. Zhou, Y. Peng, D. Sounas, X. Zhu, B. Wang, J. Dong, X. Zhang, A. Alù, and P. Lu, “Spectrum control through discrete frequency diffraction in the presence of photonic Gauge potentials,” *Physical Review Letters*, Vol. 120, No. 13, 133901, 2018.
36. Yuan, L., M. Xiao, Q. Lin, and S. Fan, “Synthetic space with arbitrary dimensions in a few rings undergoing dynamic modulation,” *Physical Review B*, Vol. 97, No. 10, 104105, 2018.
37. Yuan, L., Q. Lin, A. Zhang, M. Xiao, X. Chen, and S. Fan, “Photonic Gauge potential in one cavity with synthetic frequency and orbital angular momentum dimensions,” *Physical Review Letters*, Vol. 122, No. 8, 083903, 2019.
38. Luo, X.-W., X. Zhou, C.-F. Li, J.-S. Xu, G.-C. Guo, and Z.-W. Zhou, “Quantum simulation of 2D topological physics in a 1D array of optical cavities,” *Nature Communications*, Vol. 6, No. 1, 7704, 2015.
39. Zhou, X.-F., X.-W. Luo, S. Wang, G.-C. Guo, X. Zhou, H. Pu, and Z.-W. Zhou, “Dynamically manipulating topological physics and edge modes in a single degenerate optical cavity,” *Physical Review Letters*, Vol. 118, No. 8, 083603, 2017.
40. Luo, X.-W., X. Zhou, J.-S. Xu, C.-F. Li, G.-C. Guo, C. Zhang, and Z.-W. Zhou, “Synthetic-lattice enabled all-optical devices based on orbital angular momentum of light,” *Nature Communications*, Vol. 8, No. 1, 16097, 2017.
41. Regensburger, A., C. Bersch, B. Hinrichs, G. Onishchukov, A. Schreiber, C. Silberhorn, and U. Peschel, “Photon propagation in a discrete fiber network: An interplay of coherence and losses,” *Physical Review Letters*, Vol. 107, No. 23, 233902, 2011.
42. Regensburger, A., C. Bersch, M.-A. Miri, G. Onishchukov, D. N. Christodoulides, and U. Peschel, “Parity-time synthetic photonic lattices,” *Nature*, Vol. 488, No. 7410, 167–171, 2012.
43. Wimmer, M., A. Regensburger, M.-A. Miri, C. Bersch, D. N. Christodoulides, and U. Peschel, “Observation of optical solitons in PT-symmetric lattices,” *Nature Communications*, Vol. 6, No. 1, 7782, 2015.
44. Wimmer, M., H. M. Price, I. Carusotto, and U. Peschel, “Experimental measurement of the Berry curvature from anomalous transport,” *Nature Physics*, Vol. 13, No. 6, 545–550, 2017.
45. Chen, C., X. Ding, J. Qin, Y. He, Y.-H. Luo, M.-C. Chen, C. Liu, X.-L. Wang, W.-J. Zhang, H. Li, L.-X. You, Z. Wang, D.-W. Wang, B. C. Sanders, C.-Y. Lu, and J.-W. Pan, “Observation of topologically protected edge states in a photonic two-dimensional quantum walk,” *Physical Review Letters*, Vol. 121, No. 10, 100502, 2018.
46. Dutt, A., M. Minkov, Q. Lin, L. Yuan, D. A. B. Miller, and S. Fan, “Experimental band structure spectroscopy along a synthetic dimension,” *Nature Communications*, Vol. 10, No. 1, 3122, 2019.
47. Lustig, E., S. Weimann, Y. Plotnik, Y. Lumer, M. A. Bandres, A. Szameit, and M. Segev, “Photonic topological insulator in synthetic dimensions,” *Nature*, Vol. 567, No. 7748, 356–360, 2019.
48. Dutt, A., Q. Lin, L. Yuan, M. Minkov, M. Xiao, and S. Fan, “A single photonic cavity with two independent physical synthetic dimensions,” *Science*, Vol. 367, No. 6473, 59, 2020.

49. Yu, D., L. Yuan, and X. Chen, "Isolated photonic flatband with the effective magnetic flux in a synthetic space including the frequency dimension," *Laser & Photonics Reviews*, Vol. 14, No. 11, 2000041, 2020.
50. Malitson, L. H., "Interspecimen comparison of the refractive index of fused silica," *Journal of the Optical Society of America (1917-1983)*, Vol. 55, 1205, 1965.
51. Yuan, L. and S. Fan, "Bloch oscillation and unidirectional translation of frequency in a dynamically modulated ring resonator," *Optica*, Vol. 3, No. 9, 1014-1018, 2016.
52. Haus, H. A., *Waves and Fields in Optoelectronics*, Prentice-Hall, 1984.
53. Little, B. E., S. T. Chu, H. A. Haus, J. Foresi, and J. Laine, "Microring resonator channel dropping filters," *Journal of Lightwave Technology*, Vol. 15, No. 6, 998-1005, 1997.
54. Minkov, M., Y. Shi, and S. Fan, "Exact solution to the steady-state dynamics of a periodically modulated resonator," *APL Photonics*, Vol. 2, No. 7, 076101, 2017.
55. Gardiner, C. W. and M. J. Collett, "Input and output in damped quantum systems: Quantum stochastic differential equations and the master equation," *Physical Review A*, Vol. 31, No. 6, 3761-3774, 1985.
56. Fan, S., Ş. E. Kocabaş, and J.-T. Shen, "Input-output formalism for few-photon transport in one-dimensional nanophotonic waveguides coupled to a qubit," *Physical Review A*, Vol. 82, No. 6, 063821, 2010.
57. Saleh, B. E. A. and M. C. Teich, *Fundamentals of Photonics*, Vol. 32, Wiley, 1991.
58. Zhang, M., B. Buscaino, C. Wang, A. Shams-Ansari, C. Reimer, R. Zhu, J. M. Kahn, and M. Lončar, "Broadband electro-optic frequency comb generation in a lithium niobate microring resonator," *Nature*, Vol. 568, No. 7752, 373-377, 2019.
59. Hu, Y., C. Reimer, A. Shams-Ansari, M. Zhang, and M. Loncar, "Realization of high-dimensional frequency crystals in electro-optic microcombs," *Optica*, Vol. 7, No. 9, 1189-1194, 2020.